

Improving Visual Feature Extraction in Glacial Environments

Steven D. Morad¹, Jeremy Nash², Shoya Higa², Russell Smith², Aaron Parness², and Kobus Barnard³

Abstract—Glacial science could benefit tremendously from autonomous robots, but previous glacial robots have had perception issues in these colorless and featureless environments, specifically with visual feature extraction. Glaciologists use near-infrared imagery to reveal the underlying heterogeneous spatial structure of snow and ice, and we theorize that this hidden near-infrared structure could produce more and higher quality features than available in visible light. We took a custom camera rig to Igloo Cave at Mt. St. Helens to test our theory. The camera rig contains two identical machine vision cameras, one which was outfitted with multiple filters to see only near-infrared light. We extracted features from short video clips taken inside Igloo Cave at Mt. St. Helens, using three popular feature extractors (FAST, SIFT, and SURF). We quantified the number of features and their quality for visual navigation using feature correspondence and the epipolar constraint. Our results indicate that near-infrared imagery produces more features that tend to be of higher quality than that of visible light imagery.

Index Terms—feature extraction, glaciers, visual odometry, snow, ice, visual navigation, slam

I. INTRODUCTION

Scientific endeavors to many glaciers, such as Antarctica, are difficult and time-consuming. Extreme cold and lack of infrastructure restrict experiments. Some glaciers are littered with deadly crevasses, hidden under a deceiving layer of snow. Others break off or “calve” into the ocean, causing seismic events that register on the Richter scale. Glaciers are an environment ripe for automation.

Perception is a critical part of automation. Many machine vision algorithms rely on image features to extract meaning from an image. For navigation applications, these features are usually based on corners, regions in an image with large image gradients in two directions. Modern feature detectors find features that are invariant to camera translations and in-plane rotations. The motion of these features can inform a robot on where it is going or how the environment around it is changing – an integral part of robotics.

In our literature review, we found that a lack of visible features hamstrings robots in glacial environments. In many cases, successful glacial robots need to rely on other types of sensors. Featureless layers of snow and ice do not provide enough visual features for robotic decision making. However,

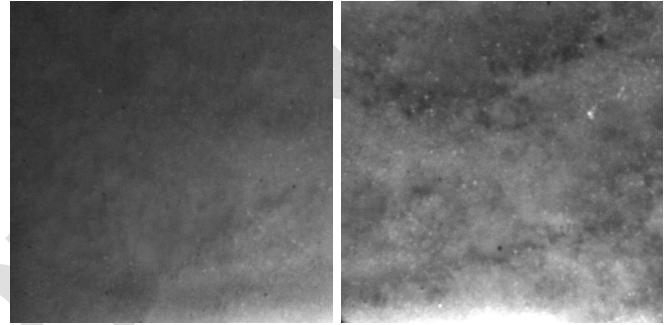
¹ Steven Morad is a graduate student in aerospace engineering at the University of Arizona, 1130 N Mountain Ave, Tucson AZ 85721, USA steven.morad@gmail.com

²Jeremy Nash, Shoya Higa, Russell Smith, and Aaron Parness are employees at the Jet Propulsion Laboratory, 4800 Oak Grove Dr, Pasadena CA 91109, USA {jeremy.nash, shoya.higa, russel.g.smith, aaron.parness}@jpl.nasa.gov

³Kobus Barnard is a professor of computer science at the University of Arizona, 1040 E 4th St, Tucson, AZ 85719, USA kobus@cs.arizona.edu



(a) The ceiling entrance to Igloo Cave



(b) Left stereo picture without a filter (c) Right stereo picture with an 800nm filter (NIR-only)

Fig. 1: Pictures from Igloo Cave at Mt. St. Helens. Both stereo pictures have contrast limited adaptive histogram equalization applied. The NIR-only image produces more and higher quality features.

glaciologists have tools to help them analyze snow and ice from afar. In particular, glaciologists make extensive use of near-infrared (NIR) light to differentiate between types of snow and ice. We leverage NIR light to improve the number and quality of visual features for machine vision applications. We investigate the optical properties of ice and snow to understand why glaciologists use this tool, and how we can adapt it for machine vision applications.

To test our hypothesis, we build a camera rig that detects both NIR and visible light, and use it to collect short video clips of Igloo Cave at Mt. St. Helens (Fig. 1). Igloo Cave is an ice cave that formed as the result of the volcanic activity of St. Helens. Our analysis of the video clips show that filtered NIR vision generally outperforms unfiltered vision in glacial environments such as Igloo Cave. We extract more features in NIR, and those features have better correspondence than in visible light.

II. RELATED WORK

A. Glacial Robots and Vision

The NASA funded Nomad robot was the first autonomous Antarctic robot. Its mission was to find meteorites in the Elephant Moraine. It was equipped with stereo cameras, but “In all conditions, stereo [vision] was not able to produce sufficiently dense disparity maps to be useful for navigation” [1].

More recently, Paton et al. mounted stereo cameras on the MATS rover to explore the use of visual odometry in polar environments. They found that feature-based visual odometry performed poorly in icy environments: “From harsh lighting conditions to deep snow, we show through a series of field trials that there remain serious issues with navigation in these environments, which must be addressed in order for long-term, vision-based navigation to succeed ... Snow is an especially difficult environment for vision-based systems as it is practically contrast free, causing a lack of visual features” [2].

Similar to Paton et al., Williams and Howard developed and tested a 3D orientation (pose) estimation algorithm on the Juneau Ice Field in Alaska. Williams and Howard wrote, “When dealing with arctic images, feature extraction is possibly the biggest challenge” [3]. They used contrast limited adaptive histogram equalization (CLAHE) post-processing to enhance contrast and make features stand out better. Their algorithm can extract many more features than previously possible, but they still experience significant pose drift.

To summarize, previous attempts at glacial robots have had less-than-successful performance with vision in icy environments. By and large, this is mostly due to lack of visual features in vast sheets of ice and snow.

B. Near-Infrared Filtering and Glaciology

Near-infrared (750-2500nm) imaging is a known tool in glaciology. Champollion used NIR imaging to get better images of hoarfrost in Antarctica [4]. NIR imagery from the MODIS satellite has been used to calculate continent-wide surface morphology and ice grain size measurements in Antarctica [5]. Matzl took NIR photographs of roughly one square meter of ice and snow, generating a 1D spatial map of grain structure within the snowpack. Matzl found that at meter-scales, differences in the snowpack are visible in NIR [6].

III. METHOD

A. Scattering Models

Wiscombe’s seminal work on the optics of snow and ice utilizes Mie theory to describe scattering. Their model describes the optics of ice and snow from 300nm to 5000nm. They find that the reflectance of ice grains between 750 and 1400nm is mostly dependent on the size of the grains [7] (Fig. 2), thereby exposing structure invisible outside those wavelengths. For reference, visible light ends at 740nm. Since their work was published, several other papers have confirmed that snow albedo (brightness) is sensitive to ice grain size in NIR wavelengths [8] [9].

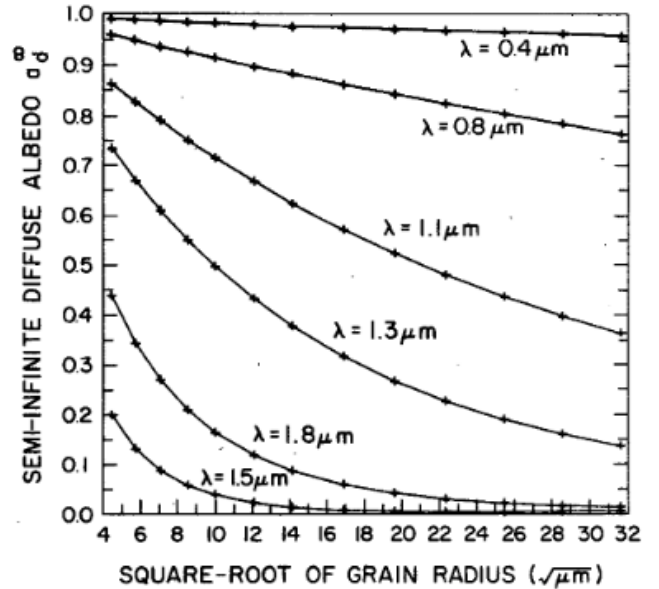


Fig. 2: NIR albedo depends much more on ice grain size than visible light. For reference, the human eye is most receptive at $0.56\mu\text{m}$ [10]. Adapted from [7], reprinted with permission.

B. Specific Surface Area and Grain Size

Ice and snow are made up of small ice crystals called ice grains, that measure from tens to thousands of microns across [5]. The term “grain size” refers to the diameter of these grains, but is sometimes misleading. In optics, the grain size of ice has two meanings: the true size of the grain or the optical size of the grain. Thus far, we have referred to the optical grain size. The optical size is used in idealized lighting models to reconcile the error between modeled and observed values for a specific true grain size.

The specific surface area (SSA) of snow and ice is defined as the ratio between the surface area and volume of the ice. SSA is strongly coupled with optical grain size [11], but can also effectively represent differences in grain shape. SSA has been shown to better represent the optical bulk-properties of real-world snow and ice [12]. The SSA can also represent spatially varying properties of snow and ice, such as air content or ice age [13]. While individual ice grains are usually too small to resolve by camera, regions of snow and ice with differing SSA are not. Varying SSA regions appear differently when viewed in NIR light. These differences in NIR light produce more visual features than if viewed in visible light.

IV. EXPERIMENT

We set out to compare the number and quality of features extracted from NIR and visible light imagery. First, we define the scenes where video is taken. Then, we discuss the camera rig design and camera parameters. We go over the video capture procedure and the metrics we use to evaluate each scene.

A. Cave Scenes

We analyze video from four different scenes inside Igloo Cave at Mt. St. Helens. The first scene is a featureless firm wall,

the second scene is a striated firm wall, and the third scene is planar snow. The fourth scene is a walking tour around one portion of the cave. Indirect sunlight illuminates all but the planar snow scene, which is illuminated by the lamp on the camera rig.

B. Camera Rig Design

A hand-held camera rig was built to collect NIR data and compare it to visible light. We mount two identical PointGrey FLEA-3 monochrome cameras to a 3D printed structure in a stereo configuration with a 10cm baseline (Fig. 3). The right camera has a filter wheel flush with the lens assembly. The filter wheel contains five NIR longpass filters with cut-on wavelengths of 800nm, 850nm, 900nm, 950nm, and 1000nm. These filters block light below their cut-on wavelength. We also attach a terrarium lamp on the underside of the rig, centered between the two cameras. The terrarium lamp has a ceramic reflector that reflects light in both visible and IR spectrums. A 75W halogen-tungsten incandescent bulb sits in the terrarium lamp to provide smooth, continuous illumination over both the visible and infrared spectrums.

C. Camera Parameters

Varying lighting conditions and the differing transmissivity of each filter made hand-setting camera parameters for each scene very difficult. Due to the significant difference in light received by the sensors, one set of parameters would not work for both cameras. By setting camera parameters differently for each camera, we could bias the results. For these reasons, we set the cameras to auto mode. Auto mode automatically sets the analog gain, shutter speed, and sharpness of each camera. Because the NIR camera receives less light, it has a higher gain and prolonged exposure, which results in noisier and blurrier video. This provides some advantage to the visible light camera, but we did not attempt to quantify the extent of the advantage.

D. Procedure

We hold the camera rig by hand and take short videos while trying to keep the rig from moving too much. In all scenes, the rig is between one and six feet from the region of interest. If the scene is too dark for the unfiltered camera, the illuminator is turned on. For each scene, we cycle through the five NIR longpass filters on the right camera. For the cave tour, the camera rig is held a few feet from the cave wall as the operator walks about the cave. The path is identical for all filters. In our videos, we observe only snow and ice. Special care is taken to ensure that no rocks or foliage appear in any of the videos. Videos that contained enough volcanic ash to affect the results were discarded, except for the full cave tour.

E. Preprocessing

Each image frame goes through a preprocessing pipeline before analysis. Lens distortion causes straight lines to appear slightly curved in the image; images are rectified to remove this effect.



Fig. 3: The camera rig and a firm wall at St. Helens

Next, we remove vignetting created by the filter wheel. Hough circles are used to detect the vignette perimeter. Once the perimeter is determined, we inscribe a bounding square in the hough circle. On both cameras, we only use data within the bounding square.

The pipeline then produces two images, an unmodified image, and an image modified with CLAHE to improve contrast, as Williams and Howard suggest [14] [3].

F. Metrics

We evaluate multiple feature detectors: SIFT [15], SURF [16], and the slightly modified scale-space version of FAST used in the ORB paper [17]. All feature detectors we use are scale-invariant by way of a scale-space pyramid. Each feature detector, except for SURF, uses default OpenCV parameters to reduce the chance of biasing parameters to improve NIR imagery at the expense of visible light imagery. The minimum Hessian threshold for SURF is raised to 500 to produce features similar in quantity and quality to SIFT and FAST.

1) *Feature Count*: The most straightforward metric is counting the number of features in each picture. Five features is the practical lower bound for visual pose estimation [18]. With RANSAC, more features result in more samples for pose estimation at the expense of some computational overhead [19]. We report the median number of features per frame over the entire video.

2) *Feature Correspondence*: Feature count can be misleading because “false features” are counted. False features are features created from camera noise or other sources that do not persist between frames and are not useful for vision. By enforcing a feature correspondence across successive image pairs, we can eliminate these false features. Correspondence also serves to enforce feature robustness to changes in camera pose. The camera is hand-held and moves slightly between frames, so features must be robust to small motion to persist through multiple frames.

We evaluate feature correspondence using epipolar geometry and the fundamental matrix F . This feature correspondence also serves to evaluate performance for visual navigation

applications, because we can deconstruct F into changes in camera pose [20].

F relates the points in two images using epipolar geometry. Let point p exist somewhere in 3D space. Let x_1 be the homogeneous pixel coordinates of p in the camera. The camera moves, and now p appears at homogeneous pixel coordinates x_2 . Then F is the matrix that satisfies the constraint $x_2^T F x_1 = 0$ [20].

In our case, p is the feature in physical space. $F x_1$ forms an epilines l_1 in the second image that p lies on. With a perfect camera, all points in image one should lie on corresponding epilines from image two. In reality, the points are usually slightly off the lines. The geometric distance of each point from its epiline can be evaluated using the Sampson distance measure [21]. If the Sampson distance is less than one (i.e. each point is within one pixel of the epiline), we consider the point as on the epiline, and the features in each image corresponding.

We use OpenCV’s RANSAC `findFundamentalMat` function [22] which requires at least eight correspondences between each pair of sequential frames to estimate the fundamental matrix F . If OpenCV can recover F and each inlier point is on the corresponding epiline, we say there is a valid correspondence for the image pair.

We count the number of valid image pairs and divide it by the total number of image pairs to find the percent of image pairs with a correspondence. The chance of a false positive correspondence is exceedingly small, which is explored in [23] in greater detail.

A score of zero percent corresponds to insufficient information for any visual navigation throughout the entire video, while a score of one hundred percent corresponds to valid camera motion between each sequential image pair.

V. RESULTS

Although we used filters up to 1000nm, indirect lighting conditions combined with reduced camera sensitivity results in pitch black videos for longer wavelength filters. We did not analyze these videos. With the illuminator on, there was enough illumination for up to 950nm. With natural indirect lighting, the maximum wavelength filter varied from 800nm to 900nm.

We provide our results in Tab. I. The overall best performing filter with regards to correspondence is 800nm. In our feature extraction test cases, 800nm filtered light outperforms unfiltered light (Fig. 4). CLAHE video usually outperforms non-CLAHE video, except when dark. Camera gain is greatly increased to compensate for darker scenes at higher wavelengths. This gain produces noise that makes CLAHE images perform worse than non-CLAHE images. This is evident by the marked increase in features, but a large decrease in correspondence. These are false features. Interestingly, 900nm without CLAHE performs reasonably well against unfiltered light with CLAHE. 900nm filters may be an appealing alternative to CLAHE for CPU-constrained robots.

TABLE I: Experimental results for each scene in Igloo Cave.

Filter	Extractor	Feat. Count	Correspondence %
Featureless firn wall			
None	FAST	0	0
	SIFT	0	0
	SURF	0	0
(CLAHE)	FAST	7	13
	SIFT	6	21
	SURF	14	98
800nm+	FAST	0	0
	SIFT	0	0
	SURF	0	0
(CLAHE)	FAST	85	64
	SIFT	90	94
	SURF	205	99
850nm+	FAST	0	0
	SIFT	0	0
	SURF	0	0
(CLAHE)	FAST	432	2
	SIFT	279	55
	SURF	484	58
900nm+	FAST	10	40
	SIFT	5	17
	SURF	10	53
(CLAHE)	FAST	500	0
	SIFT	5936	0
	SURF	1543	6
Striated firn wall			
None	FAST	0	0
	SIFT	0	0
	SURF	0	0
(CLAHE)	FAST	6	4
	SIFT	5	11
	SURF	8	26
800nm+	FAST	5	7
	SIFT	12	33
	SURF	8	33
(CLAHE)	FAST	472	0
	SIFT	4195	0
	SURF	600	0
Planar snow			
None	FAST	5	8
	SIFT	3	4
	SURF	2	0
(CLAHE)	FAST	17	69
	SIFT	11	53
	SURF	12	86
800nm+	FAST	26	100
	SIFT	5	0
	SURF	3	21
(CLAHE)	FAST	112	79
	SIFT	56	100
	SURF	74	100
850nm+	FAST	35	97
	SIFT	9	23
	SURF	7	53
(CLAHE)	FAST	210	63
	SIFT	110	100
	SURF	179	100
900nm+	FAST	34	92
	SIFT	12	69
	SURF	12	89
(CLAHE)	FAST	445	8
	SIFT	227	78
	SURF	364	83
950nm+	FAST	16	68

Filter	Extractor	Feat. Count	Correspondence %
(CLAHE)	SIFT	19	97
	SURF	23	91
	FAST	500	6
	SIFT	749	0
	SURF	655	32
Cave tour			
None	FAST	2	27
	SIFT	2	19
	SURF	2	22
(CLAHE)	FAST	45	49
	SIFT	51	60
	SURF	61	63
800nm+	FAST	0	0
	SIFT	2	5
	SURF	0	1
(CLAHE)	FAST	34	53
	SIFT	70	79
	SURF	97	82
	SURF	97	82
850nm+	FAST	0	0
	SIFT	5	19
	SURF	2	5
(CLAHE)	FAST	184	5
	SIFT	152	22
	SURF	165	42
	SURF	165	42
900nm+	FAST	3	9
	SIFT	15	72
	SURF	11	53
(CLAHE)	FAST	493	1
	SIFT	4033	0
	SURF	717	5
	SURF	717	5

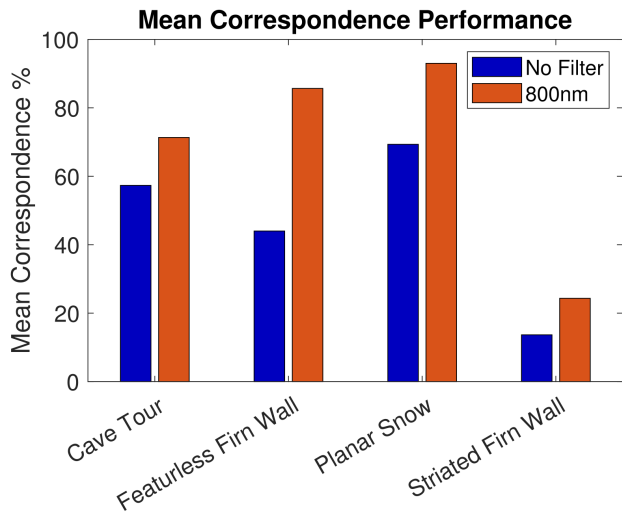
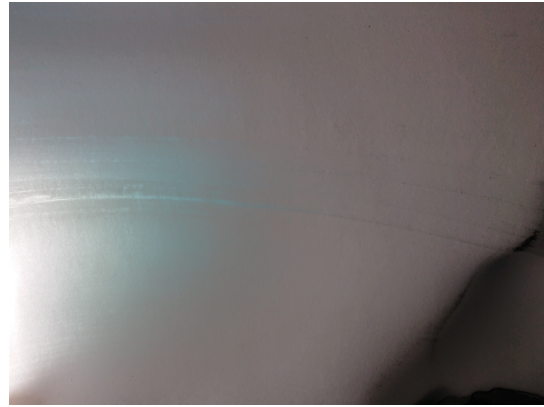


Fig. 4: Unfiltered light performance compared with the best performing (800nm) filter. We took the mean correspondence for all three feature extractors. In the four trials, NIR filtered imagery outperformed unfiltered imagery.

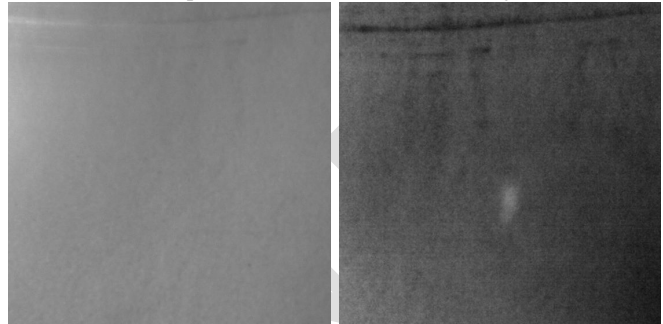
VI. DISCUSSION

A. Concrete Examples

The planar snow scene is the best example of the spatially-varying SSA. When comparing the visible light CLAHE image (Fig. 1b) to the NIR CLAHE image (Fig. 1c), there is a stark difference. The NIR CLAHE image almost looks like a cloudy sky or a nebula. The darker regions are those with smaller SSA. These are likely regions of older snow, where dendritic grains transition to round grains [24]. The brighter areas could be regions of new snow with higher SSA.



(a) Context photo of a striated firn wall in Igloo Cave



(b) Left stereo picture without a filter

(c) Right stereo picture with an 800nm filter (NIR-only)

Fig. 5: Stereo imagery of a striated firn wall. The melt-freeze crust near the top of the stereo images provides features in NIR.

Also visibly interesting is the striated firn wall scene (Fig. 5). The striation in this scene is known as melt-freeze crust, where melting snow or rain creates a layer of water, then refreezes producing large ice grains [25]. These large ice grains result in a small SSA and a dark streak in the NIR image (Fig. 5c). Note that in the unfiltered image, the SSA has little effect and the streak is barely visible (Fig. 5b).

B. Practical Considerations

While other light spectrums have interesting interactions with ice crystals, NIR light is the most practical. Most silicon CMOS and CCD camera sensors are sensitive to NIR light. Many machine vision cameras come without a NIR-blocking filter, allowing them to view NIR light out of the box. Consumer cameras tend to have NIR blocking filters to restrict the sensor to the human vision range. These filters can easily be replaced with NIR longpass filters, allowing almost any commercial camera to see in only NIR wavelengths.

While cameras sensitivities vary, the spectral sensitivity of the Flea3 cameras is representative of other commercial cameras. For most cameras, we expect that 800nm filters with CLAHE will produce the best visual features. The noisy low-light photography produced by the 900nm and higher filters combined with noise-sensitive CLAHE results in many features created from noise. A sensor that is more sensitive

to NIR light would perform better in longer wavelengths with CLAHE. Most of the testing occurred inside a darkened cave, the darker filters will likely perform better outside in direct sunlight.

C. Future Work

The cameras we used only touch the very beginning of the NIR spectrum. With specialized NIR sensors, it may be possible to extract even more features. Indium-Gallium-Arsenide sensors are commercially available and span the full NIR spectrum.

All analyzed scenes are from Igloo Cave at St. Helens. Sampling additional sites would improve the generality of our hypothesis.

Although we quantified error during correspondence, we did not quantify it in terms of physical measurement. Without scale and a ground-truth measurement of the camera motion, it is not possible to compare this error to a physical quantity. Future work on visual navigation should address this.

VII. CONCLUSION

Our experimental results from Igloo Cave suggest that NIR light is an attractive alternative to visible light for feature extraction in glacial environments. In our test cases, NIR light outperformed unfiltered light. In most cases, the 800nm filter with CLAHE performed best except for one case where the 800nm filter without CLAHE performed better. When CLAHE was not used, 900nm performed best with sufficient lighting, beating unfiltered light. The feature correspondence metric we used for comparison is tightly coupled with visual odometry methods. In snow and ice, NIR light will likely provide better visual odometry estimates than visible light due to the improved feature correspondence. Simply replacing the NIR block filter present in consumer cameras with a NIR pass filter can turn most consumer cameras into glacial vision cameras.

REFERENCES

- [1] S. Moorehead, G. Simmons, D. Apostolopolous, and W. Whittaker, "Autonomous navigation field results of a planetary analog robot in antarctica," in *Artificial Intelligence, Robotics and Automation in Space*, vol. 440, 1999, p. 237.
- [2] M. Paton, F. Pomerleau, and T. D. Barfoot, "In the dead of winter: Challenging vision-based path following in extreme conditions," in *Field and Service Robotics*, Springer, 2016, pp. 563–576.
- [3] S. Williams and A. M. Howard, "Developing monocular visual pose estimation for arctic environments," *Journal of Field Robotics*, vol. 27, no. 2, pp. 145–157, 2010.
- [4] N. Champollion, G. Picard, L. Arnaud, E. Lefebvre, and M. Fily, "Hoar crystal development and disappearance at dome c, antarctica: Observation by near-infrared photography and passive microwave satellite.," *Cryosphere Discussions*, vol. 7, no. 1, 2013.
- [5] T. Scambos, T. Haran, M. Fahnestock, T. Painter, and J. Bohlander, "Modis-based mosaic of antarctica (moa) data sets: Continent-wide surface morphology and snow grain size," *Remote Sensing of Environment*, vol. 111, no. 2-3, pp. 242–257, 2007.
- [6] M. Matzl and M. Schneebeli, "Measuring specific surface area of snow by near-infrared photography," *Journal of Glaciology*, vol. 52, no. 179, pp. 558–564, 2006.
- [7] W. J. Wiscombe and S. G. Warren, "A model for the spectral albedo of snow. i: Pure snow," *Journal of the Atmospheric Sciences*, vol. 37, no. 12, pp. 2712–2733, 1980.
- [8] A. A. Kokhanovsky and E. P. Zege, "Scattering optics of snow," *Applied Optics*, vol. 43, no. 7, pp. 1589–1602, 2004.
- [9] Y. Xie, P. Yang, B.-C. Gao, G. W. Kattawar, and M. I. Mishchenko, "Effect of ice crystal shape and effective size on snow bidirectional reflectance," *Journal of Quantitative Spectroscopy and Radiative Transfer*, vol. 100, no. 1-3, pp. 457–469, 2006.
- [10] A. Bradley, X. Zhang, and L. N. Thibos, "Achromatizing the human eye.," *Optometry and vision science: Official publication of the American Academy of Optometry*, vol. 68, no. 8, pp. 608–616, 1991.
- [11] D. L. Mitchell, "Effective diameter in radiation transfer: General definition, applications, and limitations," *Journal of the Atmospheric Sciences*, vol. 59, no. 15, pp. 2330–2346, 2002.
- [12] T. C. Grenfell and S. G. Warren, "Representation of a nonspherical ice particle by a collection of independent spheres for scattering and absorption of radiation," *Journal of Geophysical Research: Atmospheres*, vol. 104, no. D24, pp. 31 697–31 709, 1999.
- [13] L. Legagneux, A. Cabanes, and F. Dominé, "Measurement of the specific surface area of 176 snow samples using methane adsorption at 77 k," *Journal of Geophysical Research: Atmospheres*, vol. 107, no. D17, ACH–5, 2002.
- [14] S. M. Pizer, E. P. Amburn, J. D. Austin, R. Cromartie, A. Geselowitz, T. Greer, B. ter Haar Romeny, J. B. Zimmerman, and K. Zuiderveld, "Adaptive histogram equalization and its variations," *Computer vision, graphics, and image processing*, vol. 39, no. 3, pp. 355–368, 1987.
- [15] D. G. Lowe *et al.*, "Object recognition from local scale-invariant features.," in *Iccv*, vol. 99, 1999, pp. 1150–1157.
- [16] H. Bay, T. Tuytelaars, and L. Van Gool, "Surf: Speeded up robust features," in *European conference on computer vision*, Springer, 2006, pp. 404–417.
- [17] R. Mur-Artal, J. M. M. Montiel, and J. D. Tardos, "Orb-slam: A versatile and accurate monocular slam system," *IEEE transactions on robotics*, vol. 31, no. 5, pp. 1147–1163, 2015.
- [18] D. Nistér, "An efficient solution to the five-point relative pose problem," *IEEE transactions on pattern analysis and machine intelligence*, vol. 26, no. 6, pp. 0756–777, 2004.
- [19] —, "Preemptive ransac for live structure and motion estimation," *Machine Vision and Applications*, vol. 16, no. 5, pp. 321–329, 2005.
- [20] R. Hartley and A. Zisserman, *Multiple view geometry in computer vision*. Cambridge university press, 2003.
- [21] P. H. Torr and D. W. Murray, "The development and comparison of robust methods for estimating the fundamental matrix," *International journal of computer vision*, vol. 24, no. 3, pp. 271–300, 1997.
- [22] G. Bradski, "The OpenCV Library," *Dr. Dobb's Journal of Software Tools*, 2000.
- [23] F. Sur, N. Noury, and M.-O. Berger, "Computing the uncertainty of the 8 point algorithm for fundamental matrix estimation," 2008.
- [24] M. Smith and B. Jamieson, "Tracking changes in buried melt freeze crusts," in *International Snow Science Workshop, Davos, Switzerland, 2009*.
- [25] M. Smith, B. Jamieson, and C. Fierz, "Observation and modeling of a buried melt-freeze crust," in *2008 International Snow Science Workshop, Whistler, BC, 2008*, pp. 170–178.